Emission of acoustic and optical phonons by hot electrons in a two-dimensional electron system in parallel magnetic fields

W. Xu
Department of Physics, University of Wollongong, New South Wales 2522, Australia
(Received 12 October 1995; revised manuscript received 19 January 1996)

In this paper, we present a detailed theoretical study on acoustic- and optical-phonon emission by hot electrons in $Al_xGa_{1-x}As$ parabolic quantum wells in parallel magnetic fields. We consider the situation where the phonon generation is detected by phonon emission experiments. The dependence of phonon emission on the magnetic field, excitation power, and phonon emission angle has been studied through calculating the electron energy loss rate in this configuration. The main results obtained from the present theoretical study are the following. (i) In low-, intermediate-, and high-energy excitations, phonon generation is mainly through electron-phonon interaction via piezoelectric, deformation-potential, and polar-optical coupling, respectively. (ii) The strongest acoustic-phonon emission can be observed around a magnetic field at which an electronic subband becomes depopulated, and the strongest LO-phonon emission occurs around a magnetic field where the energy spacing between two subbands equals the LO-phonon energy (electrophonon resonance effect). (iii) Phonon generation in the presence of parallel magnetic fields has a different angular distribution from that at zero and perpendicular magnetic fields.[S0163-1829(96)016619-0]

I. INTRODUCTION

Phonon generation and scattering by hot electrons in low-dimensional semiconductor systems (LDSS's) have been of considerable interest[1,2] over the past two decades, due to their paramount importance in semiconductor physics and electronics and in device applications. In LDSS's, phonons provide the principal relaxation channel for excited electrons and should have a significant effect on the physical properties of the device systems. Based on phonon generation and absorption by hot electrons in LDSS's, the exploration of use of these structures as acoustical devices (e.g., high-frequency ultrasonic generators[3] and high-frequency radiation modulators[4]) will enhance the field of device applications.[5] Recent theoretical work[6,7] has demonstrated that LDSS's, such as $Al_xGa_{1-x}As/GaAs$-based heterostructures, quantum wells, quantum wires, superlattices, etc., are suitable for generating terahertz (THz) ultrasound waves based on the emission of THz acoustic phonons. State-of-the-art growth techniques, such as molecular-beam epitaxy (MBE) and metal-organic chemical-vapor deposition (MOCVD), can confine the conducting electrons in a LDSS within the nanometer distance scale, so that the energies (e.g., electronic subband energy, electron kinetic energy, Fermi energy, etc.) are on the meV scale and, consequently, the energy (frequency) of the acoustic phonons generated can reach the meV (THz) scale. Additionally, the emission and absorption of polar-optical phonons by hot electrons are very sensitive to THz electromagnetic radiation, which has been observed experimentally[8] very recently. The investigation of the generation, propagation, and detection of THz electromagnetic and ultrasonic waves has recently become an important research field because of the potential device applications. From the fact that electrons in a LDSS interact very much more strongly with phonons than with photons, one would expect that phonons may play an important role in generating and detecting THz signals.

Phonon generation can be detected experimentally by measuring the electron energy relaxation caused by electron-phonon interaction in the device system, mainly through (i) optical[9] and transport[10,11] measurements, (ii) phonon emission experiments,[2,12] and (iii) very recently, dc conductivity measurements under polarized THz radiation.[8] The experimental results obtained from (i) only give integrated information regarding the overall strength of the process of electron energy relaxation. In contrast, the phonon emission experiments measure directly the frequency and angular distribution for generating different phonon modes and, therefore, give more detailed information about the electron-phonon interaction. In (ii), the electrons are heated by a pulsed electric field and the intensity of the phonon signal is measured by using superconducting tunnel junction phonon spectrometers[12] or sensitive imaging bolometers.[13] Together with the measurement of time of flight, the generated transverse and longitudinal phonon modes can be resolved. The measurements of (iii) require[8] techniques such as free-electron lasers, and fewer results regarding electron-phonon scattering have been reported to date. Therefore, at present, the results obtained from phonon emission experiments are supposed to be the best in checking the validity of the theoretical models. On the other hand, theoretical modeling in conjunction with the phonon emission experiments will help to predict and understand the experimental findings, and this is the motivation of the present study.

Most of the experimental and theoretical studies[2] on phonon emission from a two-dimensional semiconductor system (2DSS) are focused on the case of zero[12,14,15] and/or perpendicular magnetic field.[16–18] When $B=0$, phonons are generated in the occupied electronic subbands. The intensity of the phonon signal detected increases with increasing excitation energy. At relatively low (high) input powers, the detected phonon signal comes mainly from acoustic-phonon (optical-phonon) emission. In the presence of strong perpendicular magnetic fields, Landau quantization gives the possibility to

generate phonons among the different Landau levels (LL's). At relatively low excitation levels, the dependence of acoustic-phonon generation on the magnetic field shows[17,18] a Shubnikov–de Haas type of oscillation. The acoustic-phonon emission is enhanced when the Fermi energy moves through a LL. In an $Al_xGa_{1-x}As/GaAs$-based 2DSS, when electron interaction with longitudinal optical (LO) phonons becomes a dominant process of the electron energy relaxation, the magnetophonon resonance[19] (MPR) effect can be observed by phonon emission experiments.[16] The strongest LO-phonon emission occurs at magnetic fields where the condition of MPR is satisfied. In this paper, I pay attention to the influence of a magnetic field applied parallel to the interface of a 2DSS on the phonon generation. In this configuration, the magnetic potential has the strongest coupling to the confining potential of the two-dimensional electron gas (2DEG) along the growth direction, and a hybrid magneto-electric quantization of the electronic states is formed. The electronic subband structure for different 2DSS's in parallel magnetic fields has been investigated in detail,[20,21] and the electronic properties in this situation show some interesting and unusual behaviors.[22–25] From the points of view of both fundamental study and device application, it would be valuable to study the phonon generation in this important geometry. In a 2DSS, the strong dependence of the electronic states on the parallel magnetic field offers the possibility to produce a tunable phonon generator by varying the magnetic field.

The basic difference between phonon emission and scattering by a 2DEG in parallel magnetic fields and in zero or perpendicular magnetic fields results from the following factors: (i) The electron wave function, electronic energy spectrum, and density of states (DOS) are sharply different in different configurations. (ii) The electron-phonon interaction has different characteristics in different geometries. (iii) For a 2DSS subjected to an in-plane magnetic field, the coupling of the magnetic potential to the confining potential of the 2DEG implies that the electron motion will be strongly confined, which results in an enhancement of the effective electron-phonon interaction and, consequently, in an enhanced rate of phonon generation. In Sec. II, I will look at the electronic states for a 2DSS subjected to an in-plane magnetic field. I will discuss the nature of the electron-phonon interaction in an $Al_xGa_{1-x}As$-based parabolic quantum well (PQW) structure in parallel magnetic fields in Sec. III. The results for the electronic structure and electron-phonon interaction in a 2DSS in parallel magnetic fields will be applied in Sec. III to calculate the electron energy loss rate induced by electron interaction with acoustic and LO-phonons in conjunction with the phonon emission experiments. My theoretical results for the dependence of acoustic- and LO-phonon generation on the parallel magnetic field, excitation, and phonon emission angle will be presented and discussed in Sec. IV. The main conclusions of the present study will be summarized in Sec. V.

II. ELECTRONIC STATES FOR A 2DEG IN PARALLEL MAGNETIC FIELDS

When a magnetic field is applied along the x direction (taking the xy plane as the 2D plane of a 2DEG), the electron wave function is of the kind,[21] in the Landau gauge,

$$|\mathbf{k},N\rangle = e^{i\mathbf{k}\cdot\mathbf{r}}\psi_{Nk_y}(z), \tag{1}$$

with $\mathbf{k}=(k_x,k_y)$ and $\mathbf{r}=(x,y)$, and the energy spectrum of the electron becomes[21]

$$E_N(\mathbf{k}) = \frac{\hbar^2 k_x^2}{2m_0^*} + \varepsilon_N(k_y), \tag{2}$$

where a parabolic conduction-band structure has been considered, and m_0^* is the effective electron mass. The electron wave function and the electronic subband energy along the z direction (growth direction) are determined by the one-dimensional Schrödinger equation

$$\left[-\frac{\hbar^2}{2m_0^*}\frac{d^2}{dz^2} + \frac{\hbar^2}{2m_0^*}\frac{(z-l^2k_y)^2}{l^4} + U(z) - \varepsilon_N(k_y)\right]\psi_{Nk_y}(z) = 0, \tag{3}$$

with $l=(\hbar/eB)^{1/2}$ the radius of the ground cyclotron orbit and $U(z)$ the confining potential energy of the 2DEG.

In this paper, I study the generation of phonons from a parabolic quantum well system subjected to an in-plane magnetic field. One of the main merits of this device system is that the electron wave function and the electronic subband energy can be obtained analytically, which is very convenient for further calculations of the electronic properties and, hence, allows us to get easier access to the physics considerations without involving heavy numerical calculation. The PQW defines a system such as n-i-p-i-doped semiconductors,[26] the tailoring of the conduction-band edge of a graded $Al_xGa_{1-x}As$ structure,[27] etc. The confining potential energy of this structure can be modeled by $U(z)=m_0^*\omega_0^2 z^2/2$ with ω_0 the characteristic frequency for the confinement. For a PQW structure, the electron wave function and energy spectrum are obtained, respectively, by

$$\psi_{Nk_y}(z) = \frac{1}{\sqrt{2^N N \pi^{1/2} l_B}} e^{-\xi^2/2} H_N(\xi), \tag{4}$$

with $H_N(x)$ the Hermite polynomials, and

$$E_n(\mathbf{k}) = \frac{\hbar^2 k_x^2}{2m_0^*} + \frac{\hbar^2 k_y^2}{2m_B^*} + E_N, \tag{5}$$

with $E_N=(N+1/2)\hbar\omega_B$. Here we have made the following definitions. (i) $\omega_B=\sqrt{\omega_c^2+\omega_0^2}$ with $\omega_c=eB/m_0^*$ the cyclotron frequency; $\omega_B=\omega_0$ at $B=0$. (ii) $l_B=(\hbar/m_0^*\omega_B)^{1/2}$; $l_B=l_0=(\hbar/m_0^*\omega_0)^{1/2}$ at $B=0$. (iii) $m_B^*=m_0^*[1+(\omega_c/\omega_0)^2]$; $m_B^*=m_0^*$ at $B=0$. (iv) $\xi=z/l_B-(\omega_c/\omega_B)l_B k_y$; $\xi=z/l_0$ when $B=0$. Compared with the results obtained from a PQW at zero magnetic field, we conclude that the influences of an in-plane magnetic field on the electronic structure are mainly through (1) shifting the centers of the electron wave functions by the cyclotron motion of electrons, (2) enhancing the effective electron mass along the y direction, and (3) enhancing the energy separation between different electronic subbands. These features are similar to the case[28] of a PQW wire subjected to a perpendicular magnetic field.

The free-electron Green function for a 2DEG in an in-plane magnetic field is given by

$$G_{N,\mathbf{k}}(E)=[E-E_N(\mathbf{k})+i\delta]^{-1}, \tag{6}$$

whose imaginary part is

$$\mathrm{Im}G_{N,\mathbf{k}}(E)=-\pi\delta[E-E_N(\mathbf{k})]. \tag{7}$$

Thus the density of states for electrons in the energy level N becomes

$$D_N(E)=g_s\left(-\frac{1}{\pi}\right)\sum_{\mathbf{k}}\mathrm{Im}G_{N,\mathbf{k}}(E)=\frac{1}{2\pi^2}\int d^2\mathbf{k} \times\delta[E-E_N(\mathbf{k})], \tag{8}$$

with $g_s=2$ the factor for spin degeneracy. For the case of a PQW structure, we have

$$D_N(E)=\frac{\sqrt{m_0^* m_B^*}}{\pi\hbar^2}\Theta(E-E_N), \tag{9}$$

where $\Theta(x)$ is the unit step function, and we see that the representative density-of-states effective electron mass is also enhanced by the parallel magnetic field.

The results presented above show that for a PQW structure the presence of the in-plane magnetic field will not change the 2D nature of the system.

III. PHONON EMISSION FOR A 2DSS IN PARALLEL MAGNETIC FIELDS

A. Electron energy loss rate

The results obtained from experimental[14] and theoretical[29] studies have indicated that the power signals detected in phonon emission experiments can be described by the electron energy loss rate (EELR) induced by electron-phonon interaction. The hot-electron energy loss problem in 2DSS's has been investigated rather extensively.[1,10,11,15] However, most published papers deal with the situation where the electron energy relaxations measured by magnetotransport measurements, i.e., by studying[10,11,15] the total EELR and/or the electron temperature. In phonon emission experiments, phonon signals are normally detected in a certain angle regime at fixed excitation level. Therefore, for the corresponding theoretical study, one has to consider the angular distribution of the phonon emission.

In this paper we develop a simple model to calculate the EELR in a 2DEG in in-plane magnetic fields. Using the Boltzmann equation approach, the average energy loss per unit time of an electron to the lattice, due to the electron-phonon interaction in a 2DEG in parallel magnetic fields, can be defined by[30]

$$P_T=A\sum_N\int d^2\mathbf{k}\,E_N(\mathbf{k})\left[\frac{\partial f_N(\mathbf{k})}{\partial t}\right]_{\mathrm{coll}} =A\sum_N\int d^2\mathbf{k}\,f_N(\mathbf{k})\left[-\frac{d\varepsilon}{dt}\right]_{\mathrm{coll}}, \tag{10}$$

where the presence of many electronic subbands in the structure has been taken into account, $f_N(\mathbf{k})$ is the distribution function for electrons in a state $|\mathbf{k},N\rangle$, and $A=[\Sigma_N\int d^2\mathbf{k}f_N(\mathbf{k})]^{-1}$ is the normalization factor. Applying the DOS for electrons in a 2DEG in a parallel magnetic field to the condition of electron number conservation, we have $A=1/(2\pi^2 n_e)$ with n_e the electron density of the 2DEG. In Eq. (10), $\partial f_N(\mathbf{k})/\partial t$ is the variation of $f_N(\mathbf{k})$ at time t by the scattering (collision) process, and the variation of electron energy at time t by the scattering process is in the form

$$\left[-\frac{d\varepsilon}{dt}\right]_{\mathrm{coll}}=\frac{g_s}{(2\pi)^2}\sum_{N'}\int d^2\mathbf{k}'[1-f_{N'}(\mathbf{k}')] \times[E_N(\mathbf{k})-E_{N'}(\mathbf{k}')]W_{N'N}(\mathbf{k}',\mathbf{k}), \tag{11}$$

where the scattering in the case of degenerate statistics has been included. The transition rate to scatter an electron from a state $|\mathbf{k},N\rangle$ to a state $|\mathbf{k}',N'\rangle$ is given by

$$W_{N'N}(\mathbf{k}',\mathbf{k})=W^-_{N'N}(\mathbf{k}',\mathbf{k})+W^+_{N'N}(\mathbf{k}',\mathbf{k}), \tag{12}$$

and after using Fermi's golden rule

$$W^{\pm}_{N'N}(\mathbf{k}',\mathbf{k})=\frac{2\pi}{\hbar}\sum_{q_z}\begin{bmatrix}N_Q\\N_Q+1\end{bmatrix}C_i(\mathbf{Q})G_{N'N}(q_y,q_z)\delta_{\mathbf{k}'\mathbf{k}+\mathbf{q}} \times\delta[E_{N'}(\mathbf{k}')-E_n(\mathbf{k})\mp\hbar\omega_Q], \tag{13}$$

where the upper (lower) case refers to absorption (emission) of a phonon with energy $\hbar\omega_Q$, $\mathbf{Q}=(\mathbf{q},q_z)=(q_x,q_y,q_z)$ is the phonon wave vector, and $N_Q=[e^{\hbar\omega_Q/k_BT}-1]^{-1}$ is the phonon occupation number. Further, $C_i(\mathbf{Q})$ is the square of the matrix element for an electron interacting with the ith phonon mode, and $G_{N'N}(q_y,q_z)=|\langle k_y',N'|e^{iq_zz}|k_y,N\rangle|^2$ is the form factor for electron-phonon interaction. In the presence of the parallel magnetic field the form factor depends on both q_y and q_z, because the electron wave function along the z direction is a function of k_y due to the cyclotron motion of electrons, whereas at zero and perpendicular magnetic fields the form factor depends only on q_z. The term $\delta_{\mathbf{k}',\mathbf{k}+\mathbf{q}}$ stands for the conservation of the electron momentum in the xy plane, required by the electronic structure. The term $\delta[E_{N'}(\mathbf{k}')-E_N(\mathbf{k})\mp\hbar\omega_Q]$ leads to energy conservation during an electron-phonon scattering event. After defining $\mathbf{Q}=Q(\sin\phi\cos\theta,\sin\phi\sin\theta,\cos\phi)$ in polar coordinates with ϕ the polar angle, where θ and ϕ also define the phonon emission angle, the total EELR per electron in a 2DEG in parallel magnetic fields is obtained by

$$P_T=\int_0^\infty dQ\int_0^{2\pi}d\theta\int_0^{\pi}d\phi\,P(\mathbf{Q}). \tag{14}$$

The frequency and angular distribution function for the phonon emission are given by

$$P(\mathbf{Q})=\sum_{N',N}[(N_Q+1)I^-_{N'N}(\mathbf{Q})-N_QI^+_{N'N}(\mathbf{Q})], \tag{15}$$

with

$$I^{\pm}_{N'N}(\mathbf{Q})=\frac{Q^2\omega_Q}{4\pi^4 n_e}C_i(\mathbf{Q})G_{N'N}(q_y,q_z)\sin\phi\int d^2\mathbf{k}\ f_N(\mathbf{k})[1-f_{N'}(\mathbf{k}+\mathbf{q})]\delta[E_{N'}(\mathbf{k}+\mathbf{q})-E_N(\mathbf{k})\mp\hbar\omega_Q]. \tag{16}$$

Equation (15) reflects the fact that the net energy transfer rate is the difference between phonon emission and absorption by hot electrons in the structure. In this paper, we limit ourselves to the situation where the applied electric field (or current) is low enough so that the hot-phonon effects[15] are negligible, i.e., we take the phonon temperature to be the lattice temperature.

In this paper, we use a Fermi-Dirac type of statistical energy distribution function as electron distribution through $f_N(\mathbf{k})=f[E_N(\mathbf{k})]$, where $f(x)=[e^{(x-E_F)/k_BT_e}+1]^{-1}$ with E_F the chemical potential (or Fermi energy) and T_e the electron temperature. The inclusion of electron-phonon scattering in the case of degenerate statistics implies that phonon emission occurs mainly among the occupied electronic subbands accompanied by electronic transitions around the Fermi level.

Using the electron wave function for a PQW subjected to an in-plane magnetic field the form factor for electron-phonon interaction becomes

$$G_{N'N}(q_y,q_z)=C_{N',N}\left\{\frac{l_B^2}{2}\left[\left(\frac{\omega_c}{\omega_B}\right)^2 q_y^2+q_z^2\right]\right\}, \tag{17}$$

where $C_{N,N+J}(y)=[N!/(N+J)!]y^J e^{-y}[L_N^J(y)]^2$ with $L_N^J(y)$ the associated Laguerre polynomials. After introducing the electron energy spectrum and the electron distribution function into Eq. (16), we have

$$I^{\pm}_{N'N}(\mathbf{Q})=\frac{Q^2\omega_Q}{4\pi^4\hbar^2 n_e}\left(\frac{m_0^* m_B^*}{\varepsilon_{\mathbf{q}}}\right)^{1/2}C_i(\mathbf{Q})G_{N'N}(q_y,q_z)\sin\phi\times\int_0^\infty\frac{dx}{\sqrt{x}}\ f(\varepsilon^{\pm}_{N'N}(\mathbf{Q})+x)[1-f(\varepsilon^{\pm}_{N'N}(\mathbf{Q})+x\pm\hbar\omega_Q)], \tag{18}$$

with $\varepsilon_{\mathbf{q}}=\hbar^2q_x^2/2m_0^*+\hbar^2q_y^2/2m_B^*$ and $\varepsilon^{\pm}_{N'N}(\mathbf{Q})=E_N+(E_{N'}-E_N+\varepsilon_{\mathbf{q}}\mp\hbar\omega_Q)^2/4\varepsilon_{\mathbf{q}}$.

B. Acoustic- and LO-phonon generation from an $Al_xGa_{1-x}As$ PQW

For an $Al_xGa_{1-x}As$ PQW structure, a gradual variation of the Al content along the growth direction implies that the phonon modes in the device system are very similar to those in GaAs due to the structural compatibility between GaAs and $Al_xGa_{1-x}As$. The surface phonon modes and the reflections of the phonon wave at the heterointerfaces in this structure are supposed to be much weaker than those devices such as heterojunctions and square quantum wells. Further, in phonon emission experiments, only the bulklike phonons can reach the detectors located at a fixed angle to the *xy* plane. The surface phonon modes can hardly propagate along the *z* direction. In semiconductor materials such as GaAs, electron-phonon interaction is mainly through coupling with deformation-potential acoustic phonons, piezoelectric acoustic phonons, and longitudinal optical phonons. For GaAs only the longitudinal-acoustic phonon mode is connected with the deformation potential (DP) and the square of the electron interaction matrix element is given by

$$C_{\mathrm{DP}}(\mathbf{Q})=\frac{\hbar E_D^2 Q}{2p\nu_l}\sim\omega_Q, \tag{19}$$

with E_D the deformation potential constant, ρ the density of the material, and ν_l the longitudinal sound velocity. In a zinc-blende-structure semiconductor such as GaAs, there is only one nonzero independent piezoelectric constant, $e_{14}=e_{25}=e_{36}$, and the dielectric constant κ and sound velocity are isotropic. For electron interaction with longitudinal (LP) and transverse (TP) piezoelectric phonons, the interaction matrix elements are given, respectively, by[31]

$$C_{\mathrm{LP}}(\mathbf{Q})=A_l\frac{(3q_xq_yq_z)^2}{Q^7}\sim\frac{\sin^4\phi\,\cos^2\phi\,\sin^2\theta\,\cos^2\theta}{\omega_Q}, \tag{20}$$

where $A_i=32\pi^2\hbar e^2e_{14}^2/(\kappa^2\rho\nu_i)$ with ν_i the corresponding sound velocity, and

$$C_{\mathrm{TP}}(\mathbf{Q})=A_t\frac{Q^2(q_x^2q_y^2+q_x^2q_x^2+q_y^2q_z^2)-(q_x^2q_yq_z)^2}{Q^7}\sim\frac{\sin^2\phi}{\omega_Q}[\cos^2\phi+\sin^2\phi\,\sin^2\theta\,\cos^2\theta(1-9\cos^2\phi)], \tag{21}$$

with ν_t the transverse sound velocity. In Eqs. (19)–(21) we have used the long-wavelength approximation for acoustic-phonon modes, i.e., $\omega_Q\simeq\nu_iQ$. From Eqs. (19)–(21) we note that the basic differences for electron–acoustic-phonon interaction via DP or piezoelectric (PE) coupling are (i) the DP coupling is proportional to the phonon frequency ω_Q, whereas the PE coupling is proportional to $1/\omega_Q$; and (ii) the quantity $C_{\mathrm{DP}}(\mathbf{Q})$ [Eq. (19)] does not depend on the emission angle, whereas $C_{\mathrm{LP}}(\mathbf{Q})$ [Eq. (20)] and $C_{\mathrm{TP}}(\mathbf{Q})$ [Eq. (21)] show a strong dependence on the angles ϕ and θ. For electron–LO-phonon interaction, described by the Fröhlich Hamiltonian, we have

$$C_{\mathrm{LO}}(\mathrm{Q})=4\pi\alpha L_{\mathrm{LO}}(\hbar\omega_{\mathrm{LO}})^2/Q^2, \tag{22}$$

with α the electron–LO-phonon coupling constant, $L_{\mathrm{LO}}=(\hbar/2m_0^*\omega_{\mathrm{LO}})^{1/2}$ the polaron radius, and for LO-phonons $\omega_Q\rightarrow\omega_{\mathrm{LO}}$ with ω_{LO} the LO-phonon frequency. $C_{\mathrm{LO}}(\mathbf{Q})$ does not depend on the emission angle.

In the present paper, I calculate the intensity of phonon signals measured at an angle (θ,ϕ) in a phonon emission experiment. The detected signal is the contribution of phonon emission in different vibration modes:

$$P(\theta,\phi)=P_{\mathrm{DP}}(\theta,\phi)+P_{\mathrm{LP}}(\theta,\phi)+P_{\mathrm{TP}}(\theta,\phi)+P_{\mathrm{LO}}(\theta,\phi), \tag{23}$$

where

$$P_i(\theta,\phi)=\sum_{N',N}\int_0^\infty dQ[(N_Q+1)I^{-,i}_{N'N}(\mathbf{Q})-N_QI^{+,i}_{N'N}(\mathbf{Q})], \tag{24a}$$

with

$$I^{\pm,i}_{N'N}(\mathbf{Q}) = Y_i(\mathbf{Q}) \frac{G_{N'N}(q_y, q_z)}{\sqrt{m_B^* \cos^2\theta + m_0^* \sin^2\theta}} \times \int_0^\infty \frac{dx}{\sqrt{x}} f(\varepsilon^{\pm}_{N'N}(\mathbf{Q}) + x)[1 - f(\varepsilon^{\pm}_{N'N}(\mathbf{Q}) + x \pm \hbar\omega_Q)]. \tag{24b}$$

The functional forms of $Y_i(\mathbf{Q})$ for different phonons are given, respectively, by

$$Y_{\mathrm{DP}}(\mathbf{Q}) = \frac{\sqrt{2} m_0^* m_B^* E_D^2 (\hbar\omega_Q)^3}{8\pi^4 \hbar^5 \rho \nu_l^3 n_e}, \tag{25a}$$

$$Y_{\mathrm{LP}}(\mathbf{Q}) = \frac{72\sqrt{2} m_0^* m_B^* e^2 e_{14}^2 (\hbar\omega_Q)}{\pi^2 \hbar^3 \kappa^2 \rho \nu_l n_e} \times (\sin^2\phi \cos\phi \sin\theta \cos\theta)^2, \tag{25b}$$

$$Y_{\mathrm{TP}}(\mathbf{Q}) = \frac{8\sqrt{2} m_0^* m_B^* e^2 e_{14}^2 (\hbar\omega_Q)}{\pi^2 \hbar^3 \kappa^2 \rho \nu_t n_e} \times \sin^2\phi [\cos^2\phi + \sin^2\phi \sin^2\theta \times \cos^2\theta (1 - 9 \cos^2\theta)], \tag{25c}$$

and

$$Y_{\mathrm{LO}}(\mathbf{Q}) = \frac{\sqrt{2} m_0^* m_B^* \alpha L_{\mathrm{LO}} (\hbar\omega_{\mathrm{LO}})^3}{\pi^3 \hbar^4 n_e Q}. \tag{25d}$$

For LO-phonons, $N_Q \rightarrow N_0 = [e^{\hbar\omega_{\mathrm{LO}}/k_B T} - 1]^{-1}$ and $\varepsilon^{\pm}_{N'N}(\mathbf{Q}) \rightarrow E_N + (E_{N'} - E_N + \varepsilon_{\mathbf{q}} \mp \hbar\omega_{\mathrm{LO}})^2/4\varepsilon_{\mathbf{q}}$.

IV. RESULTS AND DISCUSSION

In this paper my calculations are performed for $Al_xGa_{1-x}As$ PQW structures. In order to limit the number of parameters, I take most material parameters as those in GaAs. I use the representative density-of-states effective electron mass for GaAs at zero magnetic field ($m_0^* = 0.0665 m_e$ with m_e the electron rest mass) as the effective electron mass. The dielectric constant and the material density are taken to be $\kappa = 12.9$ and $\rho = 5.37$ kg/m^3, respectively. For GaAs, the electron–LO-phonon coupling constant $\alpha = 0.068$ and the LO-phonon energy $\hbar\omega_{\mathrm{LO}} = 36.6$ meV. Further, I take the longitudinal (transverse) sound velocity as $\nu_l = 5.29 \times 10^3$ m/s ($\nu_t = 2.48 \times 10^3$ m/s) in GaAs. It is well known[32] that the deformation potential and piezoelectric constant will be enhanced in a dimensionally reduced system. In this paper, I take $E_D = 11$ eV and $e_{14} = 2 \times 10^9$ V/m in the calculations.

The sample parameters, such as the characteristic frequency of a PQW and the electron density of the 2DEG, can be taken from the experimental data. For a model calculation, I take $\hbar\omega_0 = 8$ meV and $n_e = 6 \times 10^{15}$ m^{-2}. The chemical potential (or Fermi energy) can be determined using the condition of electron number conservation. The results obtained from the numerical calculations show that at zero and small magnetic fields, there are two occupied subbands in the system, whereas at high magnetic fields ($B > 6$ T) only the lowest subband is occupied by electrons. By varying the parallel magnetic field, one can tune the energy difference between Fermi level and subbands and between different subbands, which implies that applying a parallel magnetic field to a 2DSS can produce a tunable device.

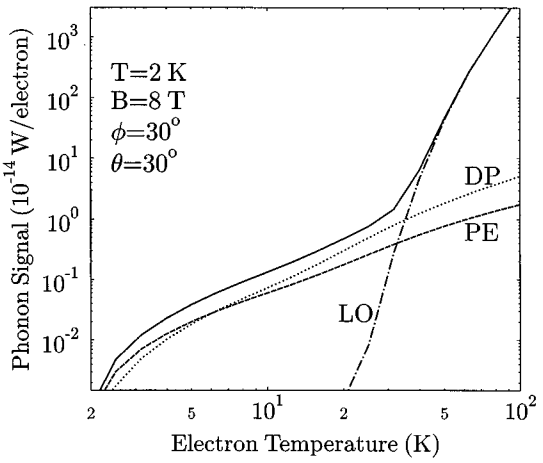

FIG. 1. Intensity of phonon signal, $P(\theta, \phi)$, as function of electron temperature at a fixed in-plane magnetic field. The contribution from electron-phonon interaction via deformation-potential (DP), piezoelectric (PE), and polar-optical (LO) coupling is presented. The solid curve is the total phonon signal detected at angle (θ, ϕ) and $P_{\mathrm{PE}}(\theta, \phi) = P_{\mathrm{TP}}(\theta, \phi) + P_{\mathrm{LP}}(\theta, \phi)$. The sample parameters are $\hbar\omega_0 = 8$ meV and $n_e = 6 \times 10^{15}$ m^{-2}.

Normally phonon emission experiments are carried out at low temperatures because of using superconducting bolometers as the phonon detectors. In the calculation I take the lattice temperature T=2 K that corresponds to using an Al bolometer as the phonon detector.[14] To calculate the intensity of the phonon signal detected, we need to know the electron temperature. In principle, the electron temperature can be calculated using the experimental data of total energy loss (P_T) which can be deduced from the applied electric field and from the sample resistivity measured at the corresponding electric field. At low lattice temperatures and low excitation levels, the relation between input power (or total energy loss) and electron temperature was predicted[33] by $P_T \sim (T_e^n - T^n)$ and in most cases[14] $n \sim 3$. At high lattice temperature and/or high excitation levels, the relation becomes[34] $P_T \sim (\hbar\omega_{\mathrm{LO}}/\tau) \exp(-\hbar\omega_{\mathrm{LO}}/k_B T_e)$ with τ the effective hot-electron relaxation time. The practical evaluation of electron temperature as a function of input power complicates the numerical calculation considerably,[29] and I do not attempt it in the present paper. As for a theoretical study I take the electron temperature (T_e) as an input parameter in the calculations.

The intensity of phonon signal detected at a fixed angle [i.e., the quantity $P(\theta, \phi)$] as a function of electron temperature is shown in Fig. 1 at a fixed parallel magnetic field. In the low-excitation-energy regime (i.e., at low electron temperatures $T_e < 5$ K), piezoelectric phonon emission is the major source of the signal. At intermediate excitation levels ($5 < T_e < 30$ K), the generation of deformation-potential acoustic phonons from the device can be observed. At high input powers ($T_e > 40$ K), the phonon signal comes mainly

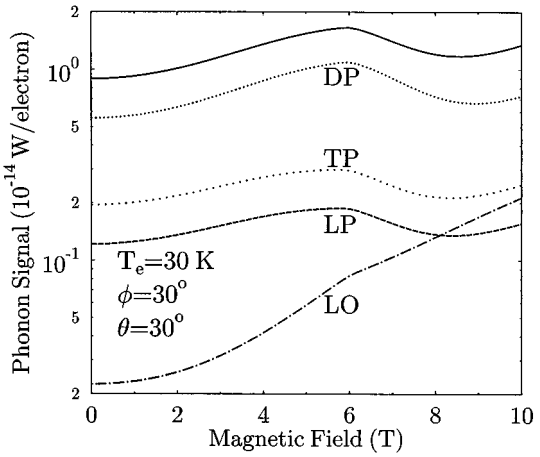

FIG. 2. Total intensity of phonon signal (solid curve) and the contribution from different phonon modes as a function of parallel magnetic field at electron (lattice) temperature $T_e=30$ K (T=2 K). The sample parameters are the same as Fig. 1.

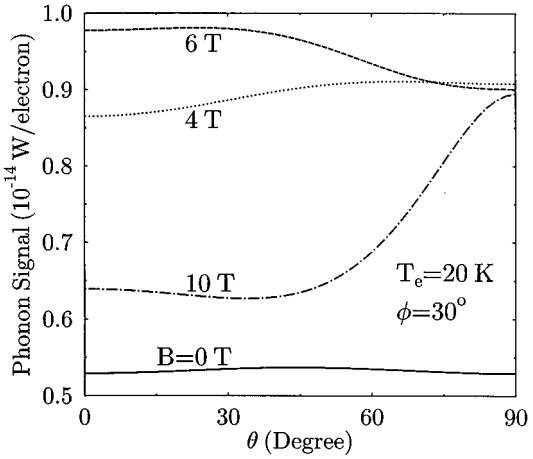

FIG. 4. Dependence of acoustic-phonon emission on the angle θ at a fixed angle ϕ for different magnetic fields. The sample parameters are the same as in Fig. 1.

from LO-phonon emission. We note that (i) these results agree with the experimental data obtained[14] for $Al_xGa_{1-x}As/GaAs$-based 2DSS's; (ii) the emission of different phonons at different electron temperatures is very similar to the resistivity (or mobility) limited by different phonon scattering at different lattice temperatures;[32] (iii) because the generated PE phonons come mainly from transverse vibration modes (see Figs. 2 and 3), the transverse acoustic (TA) phonon signals can be detected at relatively low input power; and (iv) longitudinal acoustic (LA) phonons can be measured at intermediate input powers. The results obtained from the experimental measurements[14] have indicated that for an $Al_xGa_{1-x}As/GaAs$-based 2DSS at zero magnetic field, the electron temperature $T_e=50$ K corresponds to an input power at about 5 pW/electron and when P_T is less than about 4 pW/electron acoustic-phonon emission can be detected. The PE- and DP-phonon emission at different input power regimes is a consequence of the fact that the coupling coefficient for PE phonons (DP phonons) is proportional to $1/\omega_Q$ (ω_Q), which favors the generation of low-frequency (high-frequency) acoustic phonons. Electron interaction with low-frequency (high-frequency) phonons will result in a relatively weak (strong) energy relaxation because of small (large) energy transfer. The results obtained from our further calculations show that the above-mentioned features will not be changed by varying the in-plane magnetic fields. The magnetic field will play a role mainly in varying the intensity of phonon emission detected at a fixed angle. Below, we discuss the generation of acoustic and LO phonons at different input power regimes.

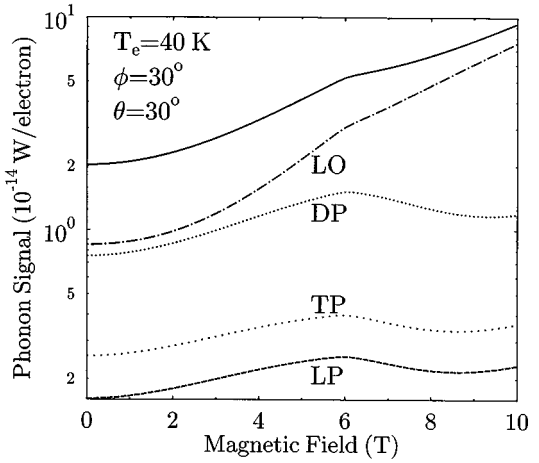

FIG. 3. Same as in Fig. 2 but for $T_e=40$ K.

A. Acoustic-phonon generation

Let us first look at the dependence of generating different phonon modes on the parallel magnetic field at a fixed angle for different electron temperatures, $T_e=30$ K (Fig. 2) and 40 K (Fig. 3). When $T_e\leqslant 30$ K, phonon emission is dominated by acoustic-phonon generation up to a high magnetic field. LO-phonon generation increases rapidly with increasing magnetic field. When $T_e\geqslant 40$ K, LO phonons are the major source of the phonon signal in all magnetic fields. From Figs. 2 and 3, we see the following. (i) The acoustic-phonon generation is enhanced by parallel magnetic fields when $B<6$ T. (ii) The strongest acoustic-phonon emission occurs around $B=6$ T where the subband $N=1$ becomes depopulated. The closing down of the scattering channel in the electronic subband $N=1$ leads to a suppression of the acoustic-phonon emission. (iii) With further increase in the magnetic field ($B>9$ T), acoustic-phonon generation can be enhanced again by the magnetic fields. (iv) The depopulation of electrons in the higher subband affects LO-phonon emission weakly due to the relatively large energy transfer for electron–LO-phonon scattering.

The dependence of acoustic-phonon emission on the angle θ is shown in Fig. 4 at a fixed angle ϕ and electron temperature for different magnetic fields. At $T_e=20$ K, the emission of DP phonons is the dominant process of phonon generation, which results in a weak dependence of the phonon generation on the angle θ at $B=0$. The angular distribution of phonon generation is determined by (i) the require-

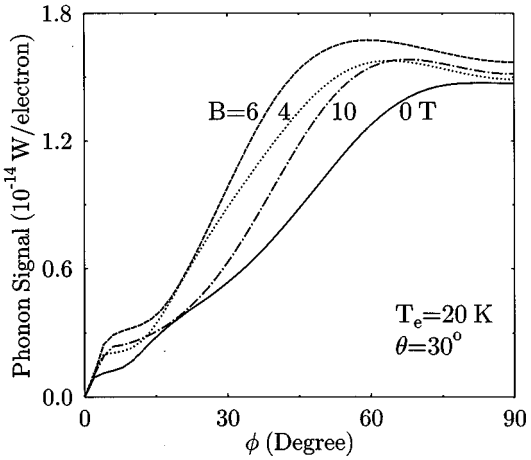

FIG. 5. Dependence of acoustic-phonon emission on the angle ϕ at a fixed angle θ for different magnetic fields. The sample parameters are the same as in Fig. 1.

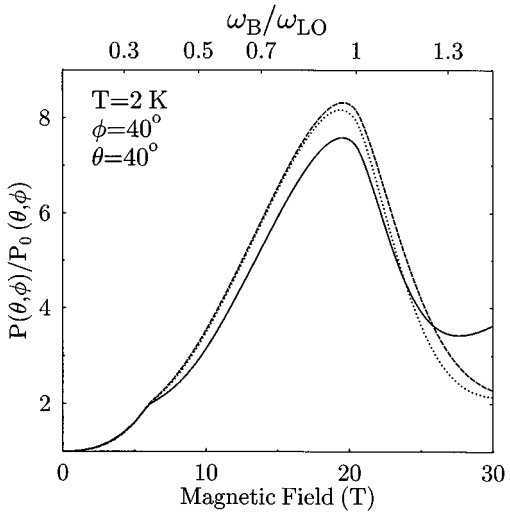

FIG. 6. Dependence of LO-phonon emission on parallel magnetic field for different electron temperatures: T_e=40 (solid curve), 50 (dotted curve), and 60 K (dashed curve). $P_0(\theta,\phi)$ is the phonon intensity at B=0. The sample parameters are the same as in Fig. 1.

ments of momentum and energy conservation during a scattering event; (ii) the electron-phonon interaction matrix element, i.e., $C_i(\mathbf{Q})$; and (iii) the form factor for electron-phonon interaction, i.e., $G_{N'N}(q_y,q_z)$. At $B=0$, the form factor depends only on q_z (i.e., on the angle ϕ) and a weak dependence of the phonon emission on the angle θ can be expected. When $B\neq 0$ the form factor is a function of $(\omega_c/\omega_B)^2 l_B^2 q_y^2$ [see Eq. (17)], which results in a strong dependence of the phonon emission on the angle θ and on the magnetic field (see Fig. 4). The nature of electron interaction with bulklike phonons implies that the form factor depends always on q_z. Thus a strong dependence of acoustic-phonon emission on the angle ϕ can be observed in all magnetic fields (see Fig. 5) and for all acoustic-phonon modes. Our theoretical results indicate that (1) a stronger acoustic-phonon emission can be observed at a larger angle θ, (2) the magnetic field will drive the emission of acoustic phonons towards a smaller-θ regime, and (iii) the TA-phonon modes can be detected at a large θ angle ($\theta>60°$).

B. LO-phonon emission: electrophonon resonance effect

From Fig. 1, we know that when the electron temperature $T_e\geqslant 40$ K LO-phonon emission is a dominant process of the electron energy relaxation and LO-phonon emission increases rapidly with T_e. The intensity of LO-phonon emission as a function of parallel magnetic field is shown in Fig. 6 at a fixed angle (θ,ϕ) for different electron temperatures, T_e=40, 50, and 60 K. To look at the net contribution of the magnetic field, we have scaled the intensity of the LO-phonon signal $P(\theta,\phi)$ by its value at zero magnetic field, $P_0(\theta,\phi)$. The effect of electrophonon resonance[35] can be clearly seen from Fig. 6. Although the oscillation in Fig. 6 is observed by varying the magnetic field, the nature of the electronic subband structure and of the DOS for a PQW subjected to in-plane magnetic fields suggests that this oscillation should be connected to the *electrophonon resonance* (EPR) effect instead of calling it *magnetophonon resonance* (MPR).[19] The basic difference between EPR and MPR is that EPR (MPR) is a consequence of electron–LO-phonon resonant scattering among the different electronic subbands (different Landau levels) and that the DOS for electrons in a system with EPR differs sharply from that with MPR. In a 2DEG, EPR occurs when the energy difference between two electronic subbands equals the LO-phonon energy, i.e., when the condition $|\varepsilon_n-\varepsilon_m|=\hbar\omega_{LO}$ is satisfied. This gives rise to a resonant electron–LO-phonon scattering between subbands n and m, and, consequently, to an enhancement of the LO-phonon generation. For a PQW subjected to parallel magnetic fields, EPR can be observed around $n\omega_B=\omega_{LO}$ with n the index difference between two subbands. Our results show that (i) when $B<20$ T LO-phonon emission increases rapidly with increasing parallel magnetic field, because ω_B increases with increasing B and the increase in ω_B leads to an approach to the condition of EPR; (ii) the strongest LO-phonon emission can be observed at about $B=20$ T where EPR occurs between subbands 0 and 1; (iii) when $B>20$ T LO-phonon emission first decreases and then increases with increasing magnetic field; and (iv) the EPR effect observed in phonon emission experiments depends weakly on the electron temperature (i.e., on the input power) in the LO-phonon emission regime. We note that although we have included five electronic subbands (i.e., $N=0\rightarrow 4$) in our calculations we cannot see the EPR oscillations at $\omega_{LO}/\omega_B=2,3,\ldots$, i.e., between subbands $0\leftrightarrow 2$, $0\leftrightarrow 3$, etc. The reasons are that our calculation is performed at low temperatures (at $T=2$ K, the contribution from LO-phonon absorption scattering is very small) and that we have used a Fermi-Dirac type of electron distribution function in the calculation. In high magnetic fields, the subbands $N\geqslant 2$ are far above the Fermi level, which will suppress the contribution to the EPR from the higher subbands.

The MPR effect has been observed in 2DSS's in strong perpendicular magnetic fields by phonon emission experiments.[16] To observe the EPR effect in the presence of parallel magnetic fields, it would be valuable to look at the LO-phonon emission angle theoretically in order to get the strongest LO-phonon signals. In Fig. 7 the intensity of the

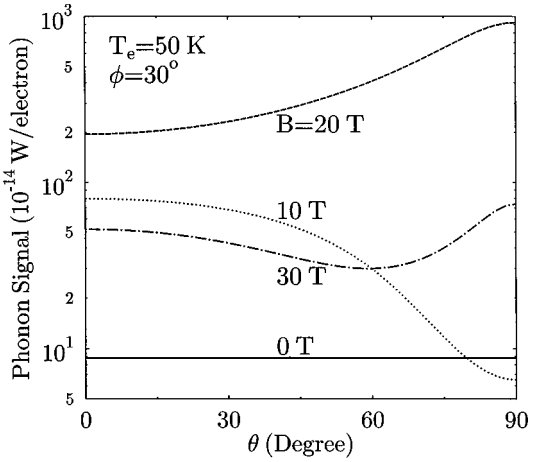

FIG. 7. LO-phonon emission angle θ at a fixed angle ϕ for different magnetic fields. The sample parameters are shown in Fig. 1.

LO-phonon signal is plotted as function of the angle θ at a fixed angle θ. At zero magnetic field, the electron–LO-phonon interaction matrix element [see Eq. (22)] and the form factor are independent of the angle θ, and so the LO-phonon emission depends very little on θ. When $B \neq 0$, the dependence of the form factor on q_y leads to a variation of the LO-phonon emission with the angle θ. Similar to the acoustic-phonon generation, the strong dependence of LO-phonon emission on the angle ϕ can be seen in all magnetic fields (see Fig. 8). The most significant conclusion we draw from Fig. 8 is that when the EPR condition is not satisfied, e.g., at $B=0$, 10, and 30 T, LO phonons are generated at large angles ϕ, whereas under the EPR condition, i.e., at $B=20$ T, LO-phonon emission be detected at almost all angles ($\phi > 10°$). This can be used for experimental measurements in order to observe the EPR effect.

To date, there is a lack of systematic experimental observation of the electrophonon resonance effect. Using transport

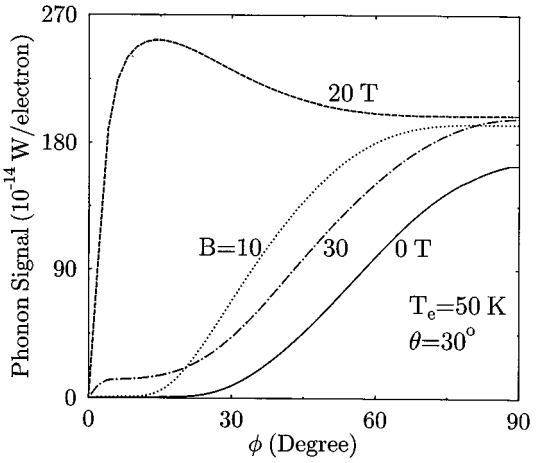

FIG. 8. LO-phonon emission angle ϕ at a fixed angle θ for different magnetic fields. The sample parameters are shown in Fig. 1.

measurements,[36] the EPR effect will be weakened considerably by electron-impurity scattering. Further, the proposed experimental methods to vary the energy spectrum of a 2DEG, such as through applying a gate voltage[36] and/or using illuminations,[37] will also vary sample parameters such as the electron density, concentration and distribution of the impurities, etc. The experimental data for the EPR effect may be smeared by these factors. It can be seen from the theoretical results presented in this paper that by combining a strong magnetic field applied parallel to the interface of a 2DSS with the measurement of phonon emission, the effect of electrophonon resonance may be observed experimentally.

V. SUMMARY

In this paper, I have studied the electronic subband structure for a two-dimensional semiconductor system in the presence of a magnetic field applied parallel to the interface of the 2DSS. Using these results, I have studied the emission of acoustic and LO phonons from an $Al_xGa_{1-x}As$ parabolic quantum well subjected to in-plane magnetic fields. I have developed a theoretical model from which the angular and frequency distribution of the phonon generation can be calculated in conjunction with phonon emission experiments. The dependence of generation of acoustic and LO phonons on the parallel magnetic field, electron energy excitation, and phonon emission angle has been studied in detail. The main results obtained from the present theoretical study are summarized as follows.

When a magnetic field is applied parallel to the interface of a 2DSS, the coupling of the magnetic potential to the confining potential of the 2DEG along the growth direction will result in a hybrid magnetoelectric quantization of electron motion. For a PQW structure, the influence of the parallel magnetic field on the electronic states is mainly through shifting the centers of the electron wave functions by the cyclotron motion of electrons, enhancing the effective electron mass and the representative density-of-states effective electron mass, and enhancing the energy separation between different electronic subbands. Nevertheless, the electrons in a PQW in parallel magnetic fields still retain their 2D nature.

The effect of the parallel magnetic field on the electron-phonon interaction in a 2DEG is mainly through varying the form factor for electron-phonon coupling. The dependence of the electron wave function on k_y gives rise to a dependence of the form factor on both q_y and q_z, which is in contrast to the case of zero and perpendicular magnetic fields where the form factor depends only on q_z.

The power signal caused by the phonon emission and detected in phonon emission experiments can be described theoretically by the electron energy loss rate induced by electron-phonon interaction. To be close to the situation of phonon emission experiments, the angular distribution of phonon emission should be considered in the calculations. A simple model, based on the Boltzmann equation approach, can be applied to calculate the EELR for a 2DEG in parallel magnetic fields and to evaluate the intensity of the phonon signal detected in phonon emission experiments.

The results obtained from my theoretical study show that (i) at low-energy excitation levels (i.e., electron temperature $T_e < 5$ K), phonon emission occurs mainly through electron

interaction with piezoelectric acoustic-phonons, (ii) at intermediate excitations (i.e., $5<T_e<40$ K), the emission of deformation-potential acoustic phonons becomes a major source of the phonon signal; (iii) at relatively high input powers (i.e., $T_e>40$ K), phonon generation is dominated by the emission of LO phonons; and (iv) the generation of TA (LA) phonons will occur at low (intermediate) input power. These features are in line with those observed experimentally. The emission of different phonons in different input power regimes will not be changed by the presence of the parallel magnetic fields.

For a 2DSS, the strong dependence of the electronic subband structure on the parallel magnetic fields offers us the possibility to observe two different types of quantum resonance effects by varying the magnetic field. At low temperatures, when the Fermi level crosses an electronic subband, quantum resonance occurs due to the closing down of the scattering channel in the depopulated subband, which is analogous to the Shubnikov–de Haas effect. At relatively high temperatures, electrophonon resonance occurs when the energy spacing between two subbands equals the LO-phonon energy, which is analogous to the magnetophonon resonance effect. In phonon emission experiments, we can observe these quantum resonance effects by exciting electrons at different electron temperatures.

In the acoustic-phonon emission regime, the strongest acoustic- phonon generation can be observed around a magnetic field at which a subband becomes depopulated. In the LO-phonon emission regime, the strongest LO-phonon emission occurs around a magnetic field where the energy difference between subbands 0 and 1 equals the LO-phonon energy $\hbar\omega_{\mathrm{LO}}$. In the presence of a parallel magnetic field, the generation of acoustic and LO phonons depends not only on the phonon emission angle ϕ but also on the emission angle θ; this is in contrast to the case of zero and perpendicular magnetic fields. The theoretical results for the angular distribution of the phonon emission will help in experimental measurements for detecting the phonon signals and observing the electrophonon resonance effect.

ACKNOWLEDGEMENT

This work is supported by the Australian Research Council.

[1] S. Das Sarma, in *Hot Carriers in Semiconductor Nanostructures: Physics and Applications*, edited by J. Shah (Academic, Boston, 1992).

[2] L. J. Challis, A. J. Kent, and V. W. Rampton, Semicond. Sci. Technol. **5**, 1179 (1990); L. J. Challis, in *Low-Dimensional Semiconductor Structures*, edited by P. N. Butcher *et al.* (Plenum, New York, 1992).

[3] See, e.g., R. M. White, in *Topics in Solid State and Quantum Electronics*, edited by W. D. Hershberger (Wiley, New York, 1972).

[4] See, e.g., X. C. Zhang, IEEE/IEOS News Lett. **7** (4), 14 (1993).

[5] See, e.g., *Ultrasonic Electronics*, special issue of Jpn. J. Phys. **33**, Pt. 1, No. 5B (1994).

[6] For the case of a 2DSS, see e.g., F. T. Vasko and V. Mitin, Phys. Rev. B **52**, 1500 (1995); F. T. Vasko, G. Balev, and P. Vasilopous, *ibid.* **47**, 16 433 (1993); W. Xu and J. Mahanty, J. Phys. Condens. Matter **6**, 6265 (1994); I. Fal'ko and S. V. Iordanskii, *ibid.* **4**, 9201 (1992); K. A. Benedict, *ibid.* **4** L371 (1992).

[7] For the case of a 1DSS, see, e.g., R. Mickevičius and V. Mitin, Phys. Rev. B **51**, 1609 (1995); R. Mickevičius, V. Mitin, V. Kochelap, M. A. Stroscio, and G. J. Iafrate, J. Appl. Phys. **77**, 5095 (1995); W. Xu, Appl. Phys. Lett. **68**, 1353 (1996).

[8] N. G. Asmar, A. G. Markelz, E. G. Gwinn, J. Č̃erne, M. S. Sherwin, K. L. Campman, P. F. Hopkins, and A. C. Gossard, Phys. Rev. B **51**, 18 041 (1995).

[9] See, e.g., R. A. Höpfel and G. Weimann, Appl. Phys. Lett. **46**, 291 (1985); C. H. Yang, J. M. Carlson-Swindle, S. A. Lyon, and J. M. Worlock, Phys. Rev. Lett. **55**, 2359 (1985).

[10] See, e.g., M. C. Payne, R. A. Davies, J. C. Inkson, and M. Pepper, J. Phys. C **16**, L291 (1983); M. E. Daniels, B. K. Ridley, and M. Emeny, Solid State Electron. **32**, 1207 (1989); K. Hirakawa and H. Sakaki, Appl. Phys. Lett. **49**, 889 (1986).

[11] Y. Ma, R. Fletcher, E. Zaremba, M. D'Iorio, C. T. Foxon, and J. J. Harris, Phys. Rev. B **43**, 9033 (1991).

[12] V. Narayanamurti, Science **213**, 717 (1981); J. C. Hensel, R. C. Dynes, and D. C. Tsui, Phys. Rev. B **28** , 1124 (1983); M. Rothenfusser, L. Köster, and W. Dietsche, *ibid.* **34**, 5518 (1986).

[13] D. C. Hurley, G. A. Hard, P. Hawker, and A. J. Kent, J. Phys. **22**, 824 (1989).

[14] For recent experimental work, see P. Hawker, A. J. Kent, N. Hauser, and C. Jagadish, Semicond. Sci. Technol. **10**, 601 (1995); P. Hawker, A. J. Kent, O. H. Hughes, and L. J. Challis, *ibid.* **7**, B29 (1992).

[15] For recent theoretical work, see S. Das Sarma, J. K. Jain, and R. Jalabert, Phys. Rev. B **41**, 3561 (1990); X. L. Lei and M. W. Wu, *ibid.* **47**, 13 338 (1994); J. R. Senna and S. Das Sarma, Phys. Rev. Lett. **70**, (2593); D. Y. Xing and C. S. Ting, *ibid.* **72**, 2812 (1994), and references therein.

[16] P. Hawker, A. J. Kent, L. J. Challis, M. Henini, and O. H. Hughes, J. Phys. Condens. Matter **1**, 1153 (1989).

[17] For experimental work, see A. J. Kent, V. W. Rampton, M. I. Newton, P. J. A. Carter, G. A. Hardy, P. Hawker, P. A. Russell, and L. J. Challis, Surf. Sci. **196**, 410 (1988); L. J. Challis, Physica B **204**, 117 (1995), and references therein.

[18] For theoretical work, see K. A. Benedict, J. Phys. Condens. Matter **3**, 1279 (1991); S. M. Badalian and Y. B. Levinson, Phys. Lett. A **155**, 200 (1991); G. A. Toombs, F. W. Sheard, D. Neilson, and L. J. Challis, Solid State Commun. **64**, 577 (1987).

[19] D. R. Leadley, R. J. Nicholas, J. Singleton, W. Xu, F M. Peeters, J. T. Devreese, J.A.A.J. Perenboom, L. van Bockstal, F. Herlach, J. J. Harris, and C. T. Foxon, Phys. Rev. Lett. **73**, 589 (1994), and references therein.

[20] J. M. Heisz and E. Zaremba, Semicond. Sci. Technol. **8**, 575 (1993); T. Jungwirth and Smrcka, J. Phys. Condens. Matter **5**, L217 (1993).

[21] W. Xu, Phys. Rev. B **51**, 9770 (1995), and references therein.

[22] T. W. Kim, M. S. Kim, E. K. Kim, and S. K. Min, Solid State Commun. **84**, 1133 (1992).

[23] G. Marx and R. Kümmel, J. Phys. Condens. Matter **3**, 8237 (1991); B. Huckestein and R. Kümmel, Phys. Rev. B **38**, 8215

(1988); J. H. Oh, K. J. Chang, G. Ihm, and S. J. Lee, *ibid.*, **48**, 15 441 (1993), and references therein.
[24] F. Piazza, L. Pavesi, H. Cruz, A. Micovic, and C. Mendoca, Phys. Rev. B **47**, 4644 (1993).
[25] A. Elci and D. Depatie, Semicond. Sci. Technol. **9**, 163 (1994).
[26] P. Ruden and G. H. Döhler, Phys. Rev. B **27**, 3538 (1983).
[27] E. G. Gwinn, R. M. Westervelt, P. F. Hopkins, A. J. Rimberg, M. Sundaram, and A. C. Gossard, Phys. Rev. B **39**, 6260 (1989); T. Sajoto, J. Jo, L. Engel, M. Santo, and M. Shayegan, *ibid.*. **39**, 10 464 (1989); I. K. Marmorkos and S. Das Sarma, *ibid.* **48**, 1544 (1993).
[28] See, e.g., H. Bruus, K. Flensberg, and H. Smith, Phys. Rev. B **48**, 11 144 (1993).
[29] W. Xu, Phys Rev. B **51**, 13 294 (1995).
[30] K. Seeger, *Semiconductor Physics*, Springer Series in Solid-State Sciences Vol. 40 (Springer, New York, 1982).
[31] X. L. Lei, J. L. Birman, and C. S. Ting, J. Appl. Phys. **58**, 2270 (1985).
[32] See, e.g., T. Kawamura and S. Das Sarma, Phys. Rev. B **45**, 3612 (1992), and detailed discussions and references therein.
[33] L. J. Challis, G. A. Toombs, and F. W. Sheard, in *Physics of Phonons*, edited by T. Paszkiewicz (Springer, Berlin, 1987), p. 348.
[34] C. H. Yang, J. M. Carlson-Swindle, S. A. Lyon, and J. M. Worlock, Phys. Rev. Lett. **55**, 2359 (1985).
[35] W. Xu, F. M. Peeters, and J. T. Devreese, J. Phys. Condens. Matter **5**, 2307 (1993); W. Xu, F. M. Peeters, and J. T. Devreese, Phys. Rev. B **48**, 1562 (1993); K. Král, *ibid.*. **50**, 7640 (1994).
[36] A. Kastalsky, F. M. Peeters, W. K. Chen, L. T. Florez, and J. P. Harbison, Appl. Phys. Lett. **59**, 1708 (1991).
[37] R. Fletcher, E. Zaremba, M. D'Iorio, C. T. Foxon, and J. J. Harris, Phys. Rev. B **41**, 10 649 (1990).